Polymer amplification to improve performance and stability towards semi-transparent perovskite solar cells fabrication

Hafez Nikbakht [a,d†], Ahmed Esmail Shalan [a†], Manuel Salado [a], Abbas Assadi [c], Parviz Boroojerdian [d]

Samrana Kazim,,[a,b] and Shahzada Ahmad,[a,b]*

[a] BCMaterials-Basque Center for Materials, Applications and Nanostructures, Martina Casiano, UPV/EHU Science Park, Barrio Sarriena s/n, Leioa 48940, Spain.

Tel: +34 946128811 Email: shahzada.ahmad@bcmaterials.net

[b] IKERBASQUE, Basque Foundation for Science, Bilbao, 48013, Spain.

[c] School of Mechanical Engineering, Maleke-Ashtar University of Technology (MUT), Isfahan 83145, Iran

[d] Department of Applied Physics, Maleke-Ashtar University of Technology (MUT), Shahin Shahr 83157-13115, Iran

[†] Authors contribute equally to the manuscript

Abstract

The performance of methylammonium lead triiodide ($CH_3NH_3PbI_3$) based solar cells depends on its crystallization and controlled microstructure. In spite of its high performance, long-term stability is a paramount factor towards its large area fabrication and potential industrialization. Herein, we have employed poly(vinylidene fluoride−trifluoro ethylene) P(VDF-TrFE) as an additive into a low concentration based perovskite precursor solutions to control the crystallinity and microstructure. Perovskite layers of lower thickness can be derived from low precursor concentration, however it often suffers from severe voids and roughness. Introducing judicious quantities of P(VDF-TrFE) can improve the surface coverage, smoothness as well as reduces the grain boundaries in the perovskite. An array of characterization techniques were utilized to probe the structural, microstructural and spectroscopic properties. Impedance spectra suggests, the P(VDF-TrFE) can improve the carrier lifetimes and reduce the charge transfer resistance, which in turn allows to improve photovoltaic performance. For an optimized concentration of P(VDF-TrFE), the fabricated semi-transparent solar cells yielded power conversion efficiency in excess of 10%, which supersede pristine devices along with improved stability. The device architect and the fabrication technique provide an effective route to fabricate cost effective and visible-light-semi-transparent perovskite solar cells.

Keywords: Perovskite solar cell; semi-transparent perovskite films; P(VDF-TrFE); microstructured control; stability.

1. Introduction

The distinctive features of organic-inorganic lead halide based perovskite allowed its usage as a promising light harvesting semiconducting pigment for photovoltaic (PV) fabrication.[1-8] The unprecedented advances in the power conversion efficiency (PCE) of perovskite solar cells (PSCs) in the current decade, has allowed it to stretch to the level of mature PV with a remarkable ~ 25.2% PCE.[9-14] Owing to the high efficiency of the perovskite based solar cells, it also provides the opportunity to fabricate semi-transparent yet efficient PV, than those based on organic or dye-sensitized solar cells.[15-17] In spite of the rapid progress in efficiency, concern on its long-term operational stability are being made, and efforts are laid to address such challenges.[18,19] Cost-effective and readily processable semi-transparent solar cells are highly attractive for building integrated PV (BIPV) application.[20] The control over microstructure and crystallinity together with uniform surface coverage of the perovskite layer is paramount for realizing high-performance, while lower thickness will allow transparency.[21] Although, reducing the thickness of the perovskite film to increase transparency is considered to be a straight path, but it brings two drawbacks: i) decreases the device performance in terms of reduced open circuit voltage (V_{oc}) and short circuit current density (J_{sc}) due to the extremely thin perovskite layers and ii) challenges in thin-film deposition with industrially adaptable process.[22-24]

To address such challenges, new growth technique for perovskite deposition was studied and various processing techniques have been reported to induce higher crystallinity. To achieve higher transparency in thin layers, different strategies such as modification of microstructure, shape and size, [25–27] or passivating the perovskite surface to detain the growth of perovskite grains [28-30] were reported. Recently, polymers were employed as an additive into the perovskite precursor solution to improve the morphology and PV performance.

In the present work, we have used ferroelectric polymer, polyvinylidene fluoride−trifluoroethylene polymer, P(VDF-TrFE) as an multipurpose agent in a low concentration for MAPbI$_3$ deposition. Its low processing temperature, rational compatibility with semiconducting materials and chemical inertness will not be a hindrance or distort the crystal structure of semiconducting materials. P(VDF-TrFE) has been used as an additive also in organic solar cells [31,32], to reduce the charge recombination and to enhance exciton dissociation and thus gave improved overall performance of fabricated solar cells. In the present work, we have employed P(VDF-TrFE) as an additive to control the crystal formation in a low precursor concentration (0.5 M) of MAPbI$_3$ for the fabrication of naked eye semi-

transparent solar cells which in turn also improves the efficiency and stability of fabricated perovskite solar cells.

The inclusion of P(VDF-TrFE) in judicious concentration, improved the surface coverage, smoothness as well as increases the crystal size, this in turn will reduces the grain boundaries in the semi-transparent perovskite layers deposited through one-step solvoneering (solvent engineering) method. It also simplifies the protocols and minimizes the approach towards semi-transparent solar cells fabrication.[33,34] Our simplified approach illustrates significantly suppressed charge recombination, improve carrier lifetimes, enhance stability and PV performance of the fabricated semi-transparent perovskite solar cells.

Experimental

Solar cell fabrication

Perovskite solar cells were fabricated using FTO (TEC15) substrates, cleaned using a sequential sonication treatment in a 2% Hellmanex solution, acetone and isopropanol, followed by UV ozone treatment for 20 min. Then samples were heated to 500 °C and a compact blocking layer of TiO_2 was then deposited onto the FTO glass substrate by spray pyrolysis, using a dilution 1/19 ml of titanium diisopropoxide bis (acetylacetonate) solution in ethanol keeping them for 30 min. Next, a mesoporous TiO_2 (30 NRD from Dyesol) was prepared by spin-coating a diluted TiO_2 dispersion in ethanol, ratio 1:8 (w/v), at 2000 rpm (1000 rpm/s acceleration) for 10 s followed by a progressive heating step till 500 °C for 30 min. The perovskite solutions were prepared inside an argon glove box under moisture and oxygen controlled conditions (H_2O level of 1 ppm and O_2 level of 10 ppm) and kept under stirring at 70 °C overnight in order to dissolve completely PbI_2. Stoichiometric precursor solutions (0.5 M) were prepared by mixing MAI (Sigma Aldrich) and PbI_2 (TCI) in dry *N, N*-dimethyl formamide (DMF, Aldrich) as described elsewhere in our previous work. The {$MAPbI_3$+ P(VDF-TrFE)} solution was prepared by adding 12 mg/mL of P(VDF-TrFE) copolymer (70:30 mol %, PiezoTech) to the 0.5 M perovskite precursor solution. The perovskite layers (with or without polymer additive) were then fabricated by using a one-step deposition process using spin-coating in two-steps mode, first step 1000 rpm for 10 s; second step 3500 rpm for 30 s. During the second step 110 µl of chlorobenzene were poured onto the films 5 s prior to the start of the program, and then substrates were annealed at 100 °C during 40 min. Once the samples were cool down to room temperature, Spiro-OMeTAD was then spun coated at 4000 rpm for 30 s by dissolving 72.3 mg of Spiro-OMeTAD in 1 ml of chlorobenzene; 17.5 µl of lithium bis-(tri-fluoro methyl sulphonyl) imide (LiTFSI) stock solution (520 mg of LiTFSI in 1 ml of

acetonitrile) and 28.8 µl of 4-tert-butylpyridine were also added to the solution as dopants. Finally, 70 nm of gold was deposited by thermal evaporation; the active area of the Au electrodes in the fabricated device was 0.16 cm^2.

Thin film Characterization

For structural characterization, thin films were prepared by spin coating of MAPbI$_3$ or {MAPbI$_3$+ P(VDF-TrFE)}onto FTO electrode. X-ray diffractograms were recorded using a D8 Advance diffractometer from Bruker (Bragg-Brentano geometry, with an X-ray tube Cu Kα, λ= 1.5406 Å). A scan range of 3–80° was selected with an acquisition time of 2 degree / min. Hitachi S-4800 scanning electron microscope was used to identify the microstructure of the synthesized materials as well as the cross-sectional imaging of the assembled solar cells. The absorption spectra were registered with an UV–Vis spectrophotometer (Varian Cary 60 Spectrophotometer). Steady state Photoluminescence (PL) measurements were recorded with a fluorescence spectrophotometer (PerkinElmer Instrument LS55).

Device characterization

Current density–voltage (*J–V*) curves were recorded with a Keithley 2400 source-measurement-unit under AM 1.5 G, 100 mW cm^2 illumination from a certified Class AAA, 450 W solar simulator (ORIEL, 94023 A). Light output power was calibrated using a NREL certified calibrated mono-crystalline silicon solar cell. A black metal mask (0.16 cm^2) was used over the square solar cell active area (0.5 cm^2) to reduce the influence of scattered light. Incident photon current efficiency (EQE/IPCE) measurements were carried out using (PVE 300, Bentham) with a xenon lamp attached to monochromator as the light source, a chopper and a calibrated silicon photodetector. Impedance Spectroscopy (IS) measurements were carried out in a Biologic SP300 system, altering the positions of the Fermi level by a white LED source. Samples were kept inside a faradaic chamber to avoid external interferences. A 20 mV perturbation in the range 2MHz–1mHz was used to obtain the spectra. After measurement, data were fitted by Z-view software in order to extract characteristic parameters of the cells.

Results & Discussions

Figure1a, represents the schematic diagram for addition of polymer in MAPbI$_3$. The derived perovskite layer embedded with the P(VDF-TrFE) will protect the perovskite layer against the

humidity and boost device performance due to surface passivation and light management. Figure 1 b and c represent the visual image of the PSCs for conventional as well as semi-transparent solar cells with P(VDF-TrFE). The devices depicts different value of transmittance and the transparency increases by decreasing the concentration of the perovskite precursor solution from {1.2 M; (Figure 1b) to 0.5 M; (Figure 1c)}. It can be deducted from the visual image (Figure 1c) that due to low precursor concentration (perovskite layer thickness ~150 nm), the spectacle background of the other side environment can be clearly seen through the light brown-coated glass as compared to photograph in Figure 1b. For the standard perovskite concentration (1.2 M, perovskite layer thickness ~400 nm), is dark brown in colour while the spectacle background appears to be blurred. Similarly, in case of thinner PSCs, in Figure S1a (0.5 M) the characters under the devices are readable by the naked eye as compared to the Figure S1b (1.2 M). Suggesting, higher transparency can be achieved using 0.5 M concentration of perovskite precursor solution; this will pave way for semi-transparent solar cell fabrication. In the current work, we focused towards the fabrication of semi-transparent perovskite solar cell and for this we deposited a lower thickness of perovskite embedded with P(VDF-TrFE) to induce stability. The transmission spectra (Figure 1d) of the two different perovskite layers with and without P(VDF-TrFE), employing similar processing protocol and solution concentrations (0.5 M), were compared with the control perovskite concentration (1.2 M). The average visible light transmission (AVT) was calculated from the transmittance value in the visible wavelength region from 450 to 750 nm as described in previous report.[35] In the case of lower concentration (0.5M) of perovskite, both spectra exhibit higher transparency at longer wavelength in the visible range (450-700 nm) as compared to control concentration (1.2 M), this will translate into clear enhancement in the transmittance of the fabricated solar cells. The semi-transparent nature in the visible-light region will give it a competitive edge, achieved due to the lower active layer thickness. The transmittance of the $MAPbI_3$ with P(VDF-TrFE) decreased and the calculated AVT value was 20% as compared to the control device with 35 % AVT (Fig.1d).
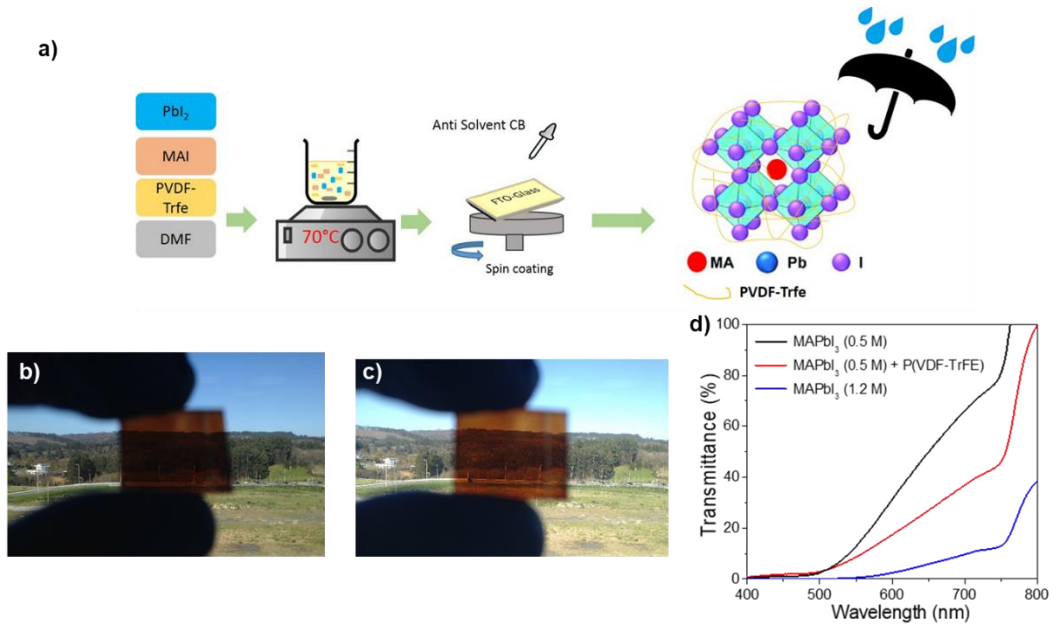
Figure 1: a) Schematic representation of polymer addition in MAPbI₃. Visual image of the perovskite layers with b) routine concentration of 1.2 M (~400 nm perovskite thickness; c) 0.5 M perovskite with P(VDF-TrFE) (~150 nm perovskite thickness showing semi-transparent effect and d) transmittance spectra of two different concentration of MAPbI₃ and with P(VDF-TrFE).

The surface coverage and microstructure of perovskite layer are influenced by P(VDF-TrFE).[36] The UV−vis and steady state PL spectra of perovskite with and without P(VDF-TrFE) are represented in Figure 2a & b. Figure 2a and b depicts slightly higher absorption and photoluminescence (PL) emission intensity of P(VDF-TrFE) added MAPbI₃ as compared to the pristine perovskite due to improved crystal growth. Slight red shift in perovskite absorption band edge with P(VDF-TrFE) inclusion can be observed which also manifest in PL spectra and can be ascribed to both the compositional change and the structural modification of the perovskite.[37] The incorporation of 12% weight ratio of P(VDF-TrFE) as additive to the perovskite solution, produces deep states in the band gap that led to an increase in the scattering of photons by the crystal defects created by the substitution, thus reducing the band gap.[37]
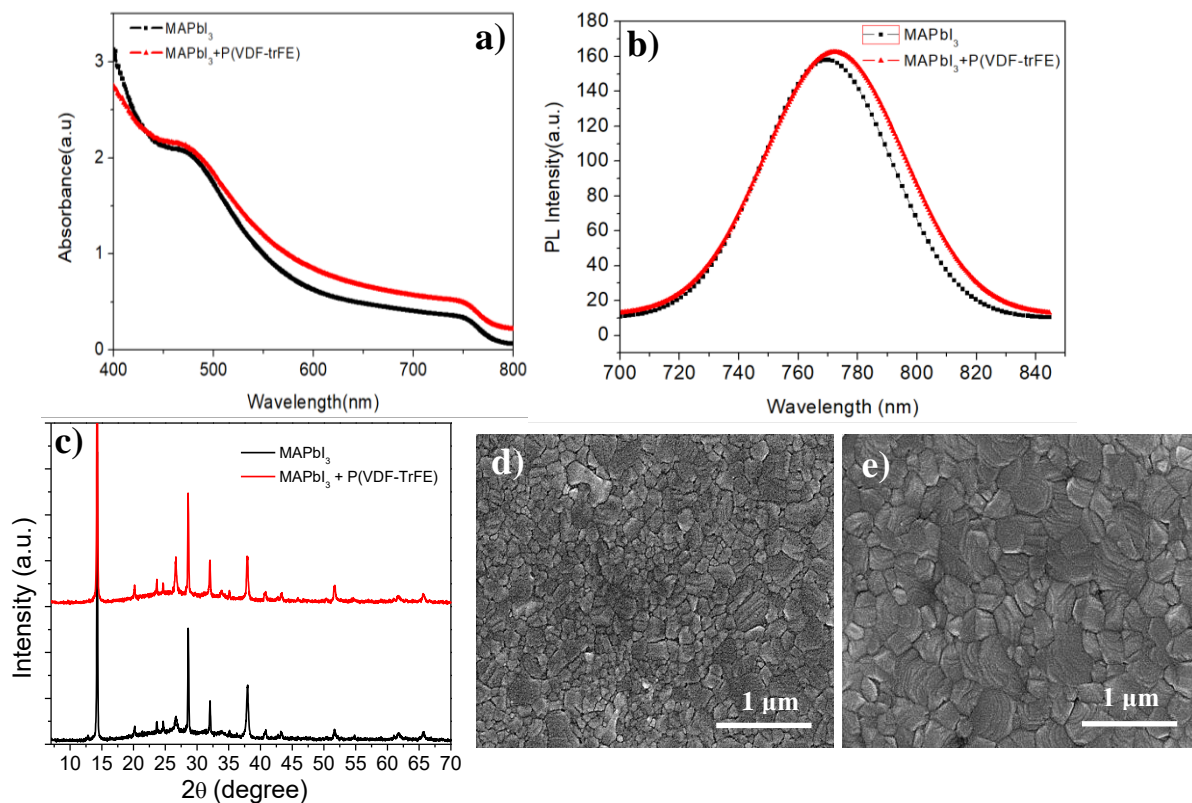
Figure 2: a) Absorption spectra and b) steady state PL spectra of MAPbI$_3$ perovskite with and without P(VDF-TrFE). c) XRD patterns of the perovskite films with and without polymer additives; SEM images of d) pristine perovskite films and e) with addition of P(VDF-TrFE) on mesoporous TiO$_2$ coated substrate.

Furthermore, the effect of P(VDF-TrFE) addition on the crystallinity of perovskite films was investigated using X-ray diffraction (XRD) as shown in Figure 2c. The diffractograms show a tetragonal perovskite structure with high phase purity and is in accordance with the earlier reports.[38,39] The peaks at 14.21°, 28.49°, and 31.95° can be assigned to the perovskite (110), (220), and (310) planes, respectively; corresponding to the tetragonal crystal structure of CH$_3$NH$_3$PbI$_3$.[37] The intensity of these assigned peak in perovskite increases in the presence of P(VDF-TrFE), which points its role in inducing high degree of crystallinity. This can be ascribed to the delay in PbI$_2$ crystallization by the addition of P(VDF-TrFE), which enhance the interaction between PbI$_2$ and MAI to allow formation of MAPbI$_3$ with improved crystallization due to the ferroelectric properties of the polymer.[40] The diffraction peaks at 37.88° corresponds to the FTO substrate.
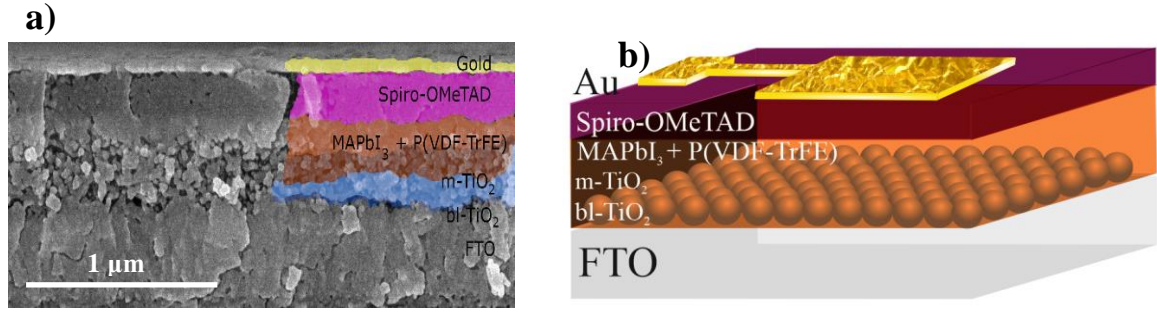
Figure 3: a) Cross-sectional image and b) configuration of the device having the structure of [FTO/bl-TiO$_2$/mp-TiO$_2$/perovskite+ P(VDF-TrFE) ~150 nm/HTM/Au].

Another advantage of P(VDF-TrFE) inclusion to the perovskite matrix is to improve the microstructure of the perovskite, and thus optimize the PV performance. The SEM surface topography images the pristine perovskite and with P(VDF-TrFE) are illustrated in Figure 2d and e. It can be noted from Figure 2 d and e, the lateral size of crystal grains increases by P(VDF-TrFE) addition to the perovskite precursor solution. The pristine perovskite microstructure is composed of many small irregular crystals (Figure 2d). By the usage of P(VDF-TrFE), we have noted improved surface coverage with no voids along with enhancement in the crystal size. Furthermore, the introduction of P(VDF-TrFE), interconnects the adjacent grains and thus grain boundary interfaces became invisible with significantly reformed microstructure. These findings are consistent with the XRD results. The mechanism to produce smooth and high-crystallinity perovskite film in the presence of ferroelectric semiconducting polymer such as P(VDF-TrFE) is still not clear yet, but it may be related to the transformation in the reaction and/or crystallization kinetics of the MAPbI$_3$ film doped with P(VDF-TrFE).[36]

The perovskite solar cells were fabricated using a one-step solution process, with a conventional mesoporous architecture of FTO/(bl-TiO$_2$)/(mp-TiO$_2$)/MAPbI$_3$ [pristine and with P(VDF-TrFE)]/Spiro-OMeTAD/Au in order to gaze the influence of ferroelectric polymer on the PV performance. The corresponding schematic diagram and cross-section SEM of the fabricated solar cell with P(VDF-TrFE) is illustrated in Figure 3a and b. The thickness of the prepared pristine perovskite layer and with P(VDF-TrFE) additives was approximately around 150 nm. We have noted that P(VDF-TrFE) addition decreases the film roughness significantly. To guide the eye, each layer has been represented by different colour for identification.

Table1: Photovoltaic parameters of J_{sc}, V_{oc}, FF and PCE of perovskite solar cells (0.5 M) and with *P(VDF-TrFE)*.

Devices[a]	J_{SC} /mA cm^{-2} [b]	V_{OC} /mV [b]	FF [b]	PCE% [b]
MAPbI₃ + P(VDFTrFE)	17.43 (15.51±1.04)	885 (930±30)	0.664 (62.02±3.94)	10.20 (8.86±0.57)
MAPbI₃	15.25 (14.58±0.84)	952 (900±30)	0.629 (62.26±3.48)	9.15 (8.17±0.54)

[a] The devices were fabricated using perovskite solution (0.5M concentration) with and without polymer P(VDF-TrFE) additives. [b] The average values shown in parentheses were obtained from 20 devices fabricated under the same experimental conditions for each perovskite solution.
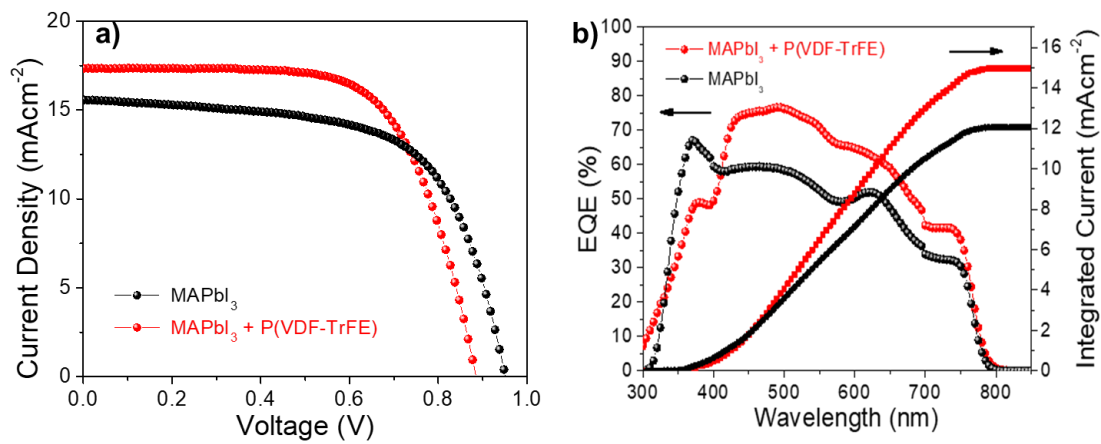

Figure 4: a) $J-V$ curves of the MAPbI₃ and with P(VDF-TrFE) based devices under AM 1.5 illumination and b) the corresponding EQE responses as well as the integrated J_{sc} of the devices of MAPbI₃ with and without P(VDF-TrFE).

The PV parameters and the *J-V* curves for the best devices prepared with and without P(VDF-TrFE) are summarized in Table 1 and Figure 4a, respectively. Table 1 shows the mean values and standard deviation calculated from the results for 20 individual devices. The results (Table 1) indicate the short-circuit current density (J_{sc}), the fill factor (FF) show increment and thus the PCEs increases significantly with the use of P(VDF-TrFE). The PV parameters values for the two samples with and without P(VDF-TrFE) were 17.34, 15.25 mAcm^{-2}; 0.885, 0.952 V; 66.44, 62.98 % and 10.20, 9.15 % for J_{sc}, V_{oc}, FF and PCE, respectively. It can be noted that the enhancement in PCE values for the optimized samples with polymer was almost 20% than that of the pristine ones due to its higher crystallinity, indicating positive effect on the efficiency of the fabricated solar cells. The external quantum efficiencies (EQEs) were also recorded [36,37] and the results are in accordance with the absorption spectra, particularly in the wavelength region of 400 - 800 nm, specifies the contribution (Figure 4b) from P(VDF-TrFE).

This enhancement in the EQE results is consistent with the J_{sc} results obtained. In addition, the integrated J_{sc} values (15.2 and 12.1 mA/cm^2 cells with P(VDF-TrFE) and pristine respectively) calculated from the EQE data is in agreement with J-V curves (Figure 4b). Slight mismatch can be noted between the original and integrated data, which may have resulted from the decay of the cells during the measurements outside the glovebox or the mismatch between the photon flux AM 1.5 G spectrum and the solar simulator. Due to uncontrolled and irrational crystal formation, hysteresis behaviour can be observed, which influence the solar cells actual performance. The negative starting bias of forward scan would weaken the efficiency, while the positive starting bias of reverse scan would enhance the performance. We have measured the devices in both forward and reverse direction (after 3500 hours) to note any such discrepancies. Slight drop in the J_{sc} was observed (Figure S2), which can be mainly due to ageing of devices (measured after 3500 hours) or voltage-settling interval that can discriminate the small difference in capacitive current.[35,41,42] Table S1 summarizes the PV parameters J_{sc}, V_{oc}, FF and PCE of the devices fabricated using perovskite solution (0.5M concentration) with and without P(VDF-TrFE) in both forward and reverse direction to evaluate hysteresis behaviour.

In order to evaluate the stabilized power output of devices, they were subjected to maximum power point (MPP) tracking for 300 s (Figure S3). The devices follow the similar trend and P(VDF-TrFE) based devices gave improved results as compared to the pristine MAPbI$_3$.

Statistical analysis of the performance parameters with mean values and standard deviation of all the assembled 20 individual devices with detailed data were summarized in Tables S2-S3. The mean PCEs of the devices fabricated with P(VDF-TrFE) and pristine are shown in Figure 5a and values were 10.20 (8.86 ± 0.57), and 9.15 (8.17 ± 0.54)%, respectively. Furthermore, the mean of other parameters J_{sc}, V_{oc} and FF for the same devices were shown in Figure S4 (a-c). The results exhibits minute standard deviation in the PV parameters, suggesting P(VDF-TrFE) positive role in improving not only the PV performance, but also the reproducibility. The long-term stability of the fabricated devices, pristine as well as with P(VDF-TrFE) was evaluated either inside glovebox under argon atmosphere or outside glovebox in ambient air (RH 50%). The stability measurements for the devices kept at ambient air are shown in Figure 5b, while for the devices which were kept inside glovebox are shown in Figure S5. The results demonstrate improved stability over a period ~150 days (> 3500 h) and maintained ~85% of their initial performance in both the cases. This can also be an indicator of positive effect on the life time by the use of P(VDF-TrFE) in perovskite solar cells. Our results thus not only suggests the semi-transparent nature of perovskite solar cells but also

the improved performance and competitive stability to put forward these devices as excellent candidate for semi-transparent PV applications.
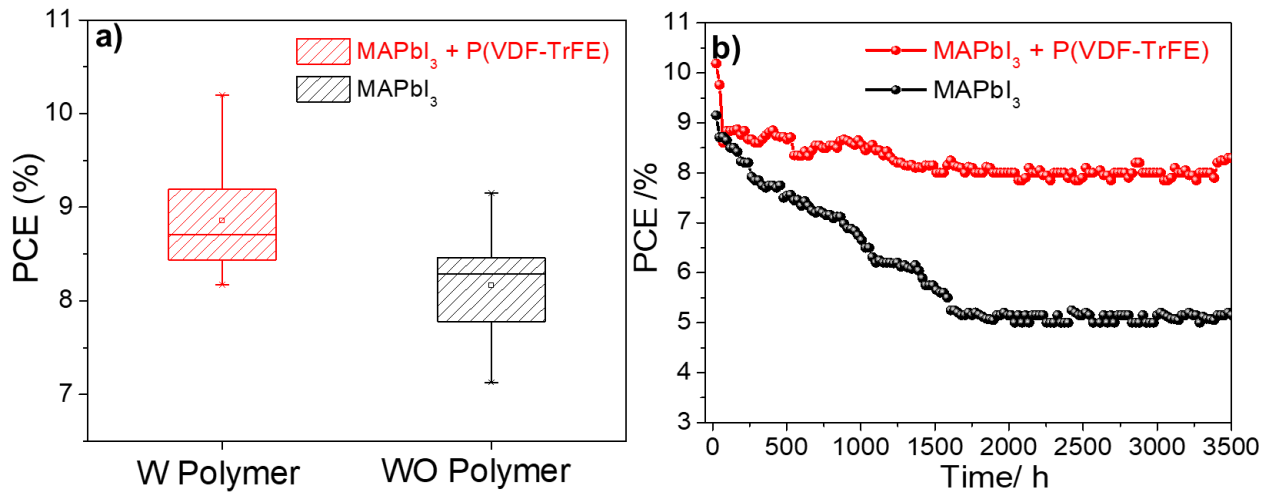

Figure 5: a) Statistics analysis of power conversion efficiencies in the form of box charts and b) PCE monitored for extended period of time and the solar cells were kept in atmospheric environment (50%RH) for stability evaluation.

To unravel the plausible reason for improved stability in the fabricated solar cells, possibly originated due to enhanced hydrophobic and moisture blocking property with the addition of P(VDF-TrFE) into perovskite matrix, we performed contact angle measurements (Figure 6). As, intended the contact angle value for the P(VDF-TrFE) amplified perovskite layer increased significantly to 91.2° from 69.8° for pristine. We have also noted, the contact angle value remains constant over the period of time (30 s). This suggest an increase in the moisture tolerance behavior of modified perovskite layers and confirm the improve stability achieved (Fig.5), due to value-added surface hydrophobicity of P(VDF-TrFE).
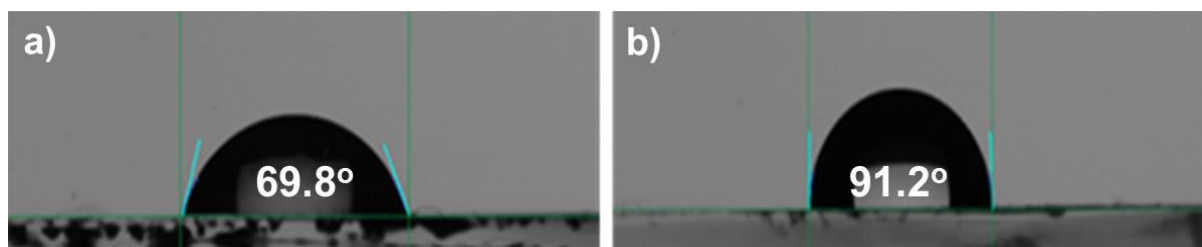

Figure 6 : Contact angle measurements of the samples a) without and b) with P(VDF-TrFE) as an additive in perovskite layers. The measurements were performed by water droplet dropping on perovskite layers. The resulted angle is the average of three different measurements at different place, and each measurement have been made at t=0 min, while putting the water droplet and after 30 sec from the drop fall.

Further, to gain insight into the charge separation and extraction, the steady-state PL spectra of pristine perovskite films coated with Spiro-OMeTAD and with P(VDF-TrFE) modified perovskites were performed on quartz substrates (Figure 7). The PL of perovskite films is expected to occur due to the recombination of localized excitons, which exist in the perovskite domain. The spectra of Quartz/MAPbI$_3$-P(VDF-TrFE)/Spiro-OMeTAD shows a significant quenching in PL as compared with pristine perovskite based samples, indicating that the charge carriers generated in MAPbI$_3$ can be efficiently separated and extracted.

The high PL quenching in the P(VDF-TrFE) based perovskite layers indicates that most of the free carriers generated by illumination are efficiently separated and transferred to Spiro-OMeTAD and the recombination of these free carriers were greatly suppressed, which is ascribed to the improved crystallinity and grain boundaries as compared to the pristine perovskite. Thus, the short-circuit current J_{sc}, *FF* and thus PCEs were improved for the P(VDF-TrFE) based samples, (Table 1), due to the ferroelectric properties of P(VDF-TrFE) which can enhance the charge separation and retract the charge recombination in these cells.
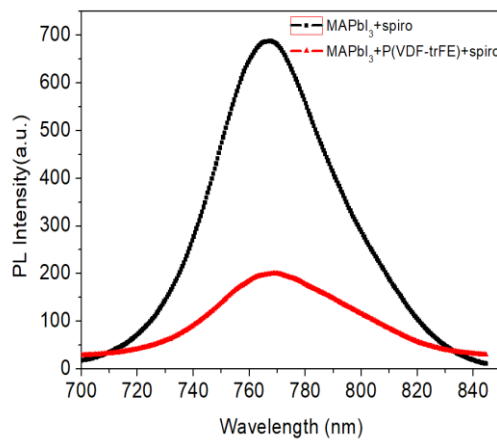

Figure 7: Steady state PL spectra of quartz/perovskite/Spiro-OMeTAD with and without P(VDF-TrFE)

In order to unravel the influence on charge dynamics of P(VDF-TrFE) addition, we characterized them by electrochemical Impedance Spectroscopy (EIS) under illumination. EIS allow us to obtain information about internal processes occurring in PSCs such as recombination resistance, charge transport resistance and ionic processes. We have observed that the incorporation of the P(VDF-TrFE) in the perovskite structure induce an improvement in the current density. Therefore, we suggest that there exists a change in the recombination mechanism inside the MAPbI$_3$ structure due to, e.g, grain boundaries passivation.

It is worth to mention the competitive performance of fabricated devices in spite of lower concentration of reactants (0.5 M). Which will allow forming thin capping atop of the

mesoporous layer, e.g, the majority of the perovskite layer is infiltrated in mesoporous nanoparticles. Although (Fig. S6 a & b) the complex impedance (Nyquist) plot obtained is in accordance with previous results which are typically represented by two or three features (arcs). In this work, two arcs with different characteristic frequencies can be distinguished for all the analyzed devices.[40,43] Those two processes can be observed more clearly in Bode representation (Fig. 8 a and b). In case of devices with P(VDF-TrFE), slower charge processes were observed (10^1-10^2 Hz), which suggest a different recombination mechanism. Therefore, in order to elucidate further information about the kinetics of the devices from impedance data, we fit the spectra by means of a simple equivalent circuit. In this circuit, R_s is the series resistance, R_{mf}, R_{lf} correspond to the resistance and C_{mf} and C_{lf} are the capacitance at medium and low frequency respectively. Therefore, fitting parameters such as recombination resistance, capacitance and their product time constants ($\tau_{mf} = R_{mf} * C_{mf}$) can be extracted.
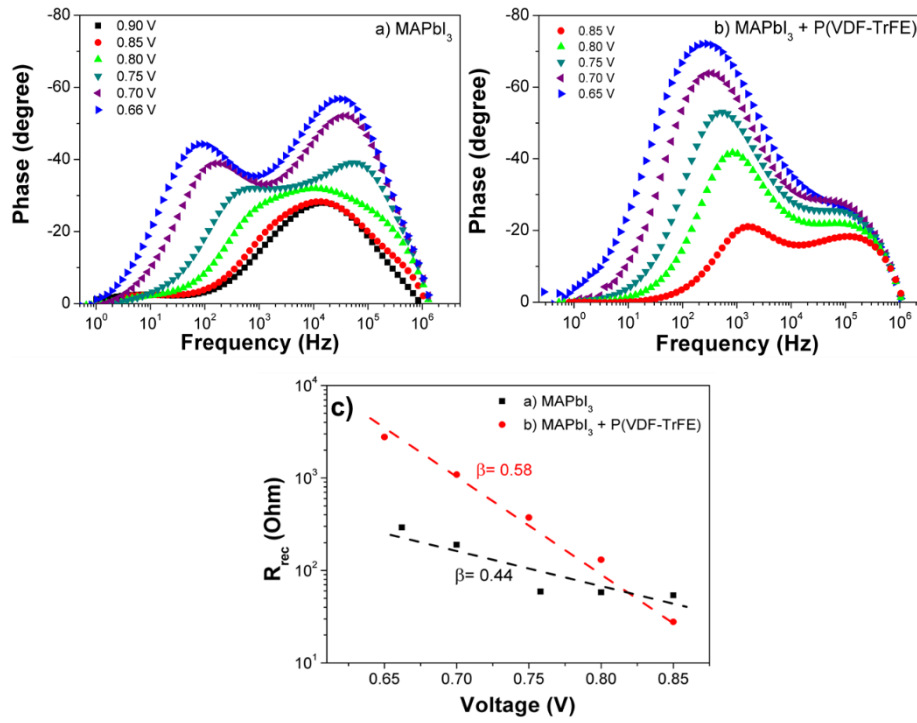

Figure 8: Bode plot of solar cell with a) pristine MAPbI$_3$, with b) P(VDF-TrFE) and c) recombination resistance as a function of voltage along with β–parameter.

According to previous reports, [44] recombination process determines the open-circuit voltage, and it is governed by the bulk of the perovskite layer via a trap-limited mechanism. In addition, following the hypothesis and the mathematical development involved in this work, it is possible to determine any change in recombination processes in the perovskite layer with the addition

of P(VDF-TrFE). Figure 8c shows indeed that the recombination resistance as extracted from the open-circuit impedance experiment follows an exponential law with respect to open-circuit potential. As aforementioned, processes appearing at different time-scale induce a change in charge dynamic of the solar cells. As it can be seen in the graph, the addition of the P(VDF-TrFE) induces a change (slope) in the recombination mechanism. From the slope, the β-parameter as well as the ideality factor can be extracted. In the case of control samples, the results are in accordance with previous studies, with an ideality factor close to 2, suggesting bulk recombination mechanism. However, with the addition of the P(VDF-TrFE) in the structure, the calculated ideality factor is close to 1.5. This indicate an influence of the P(VDF-TrFE) in the grain boundaries, such as passivation process or reduction in the grain boundaries. We speculate improved crystal formation due to a slow-down of the crystal growth together with an efficient charge extraction are the plausible cause of enhance performance.

Conclusions

P(VDF-TrFE) incorporation was found to control the crystal growth in semi-transparent perovskite layers having thickness of ~150 nm. The P(VDF-TrFE) added perovskite layer shows improved microstructure, high surface coverage, large crystal size and reduced grain boundaries as compared to the pristine $MAPbI_3$. This reform microstructure was in all like hood due to the slower transformation from the precursors to $MAPbI_3$ induced by the P(VDF-TrFE) incorporation. As compared with the pristine $MAPbI_3$ which yielded an efficiency of 9.15%, an improvement in the average PCE was observed by the addition of P(VDF-TrFE) and registered a competitive 10.20% efficiency for semi-transparent solar cells. The plausible reason behind this phenomenon comes from the improvement occurs for the separation of photogenerated carries through the fine crystallinity, improve carrier lifetimes and decreasing the charge transport resistance in the fabricated devices. The added advantage of P(VDF-TrFE) in the perovskite matrix is to obtain high-quality semi-transparent perovskite films with low thickness, improved stability which will pave the way to wide applications in building integrated photovoltaics field.

Conflicts of interest

The authors declare no conflict of interest.

Acknowledgements

References

[1] A. Kojima, K. Teshima, Y. Shirai, T. Miyasaka, *J. Am. Chem. Soc.* **2009**, *131*, 6050−6051.

[2] H. S. Kim, C. R. Lee, J. H. Im, K. B. Lee, T. Moehl, A. Marchioro, S. J. Moon, R. Humphry-Baker, J. H. Yum, J. E. Moser, M. Grätzel, and N.-G. Park, *Sci. Rep.* **2012**, *2*, 591−597.

[3] M. M. Lee, J. Teuscher, T. Miyasaka, T. N. Murakami, H. J. Snaith, *Science* **2012**, **338**, 643−647.

[4] J. Burschka, N. Pellet, S. J. Moon, R. Humphry-Baker, P. Gao, M. K. Nazeeruddin, M. Grätzel, *Nature* **2013**, *499*, 316−319.

[5] J. H. Heo, S. H. Im, J. H. Noh, T. N. Mandal, C.-S. Lim, J. A. Chang, Y. H. Lee, H.-J. Kim, A. Sarkar, M. K. Nazeeruddin, M. Grätzel, S. I. Seok, *Nat. Photonics* **2013**, *7*, 486−491.

[6] A.^^D. Jodlowski, C.^^R. Carmona, G. Grancini, M. Salado, M. Ralaiarisoa, S. Ahmad, N. Koch, L. Camacho, G.^^D. Miguel, M.^^K. Nazeeruddin, *Nat. Energy* **2017**, *2*, 972</jnl>.

[7] F. Giustino, H.^^J. Snaith, *ACS Energy Lett.* **2016**, *1*, 1233--1240.

[8] S. Kazim, M. K. Nazeeruddin, M. Grätzel, S. Ahmad, *Ang. Chem. Int. Ed.* **2014**, *53*, 2812-2824; *Angew. Chem.* **2014**, *126*, 2854--2867

[9] M. Salado, A. D. Jodlowski, C. R.-Carmona, G. de Miguel, S. Kazim, M. K. Nazeeruddin, S. Ahmad, *Nano Energy,* **2018**, *50*, 220-228.

[10] L. Calió, S. Kazim, M. Grätzel, S. Ahmad, *Angew. Chemie - Int. Ed.* **2016**, *55*, 14522-14545; *Angew. Chem.*, **2016**, *128*, 14740-14764.

[11] H. Zhou, Q. Chen, G. Li, S. Luo, T.-B. Song, H.-S. Duan, Z. Hong, J. You, Y. Liu, Y. Yang, *Science* **2014**, *345*, 542−546.

[12] J. You, Z. Hong, Y. Yang, Q. Chen, M. Cai, T.-B. Song, C.-C. Chen, S. Lu, Y. Liu, H. Zhou, Y. Yang, *ACS Nano* **2014**, *8*, 1674−1680.

[13] G. Hodes, *Science* **2013**, *342*, 317−318.

[14] S. Patra, N. Munichandraiah, *J. Appl. Polym. Sci.* **2007**, *106*, 1160−1171.

[15] S. Ahmad, E. G. Rodriguez, L. Kavan, Michael Grätzel, M. K. Nazeeruddin *Energy Environ. Sci.,* **2013**, *6*, 3439 -3466.

[16] Y.-F. Chiang, R.-T. Chen, A. Burke, U. Bach, P. Chen, T.-F. Guo, *Renewable Energy* **2013**, *59*, 136–140.

[17] C.-C. Chueh, S.-C. Chien, H.-L. Yip, J. F. Salinas, C.-Z. Li, K.-S. Chen, F.-C. Chen, W.-C. Chen, A. K.-Y. Jen, *Adv. Energy Mater.* **2013**, *3*, 417–423.

[18] F. Bella, G. Griffini, J.-P. Correa-Baena, G. Saracco, M. Grätzel, A. Hagfeldt, S. Turri, C. Gerbaldi, *Science,* **2016***, 354*, 203–206.

[19] Z. Wang, Z. Shi, T. Li, Y. Chen, W. Huang, *Angew. Chem. Int. Ed.* **2017**, **56**, 1190–1212.

[20] D. Bae, A. Palmstrom, K. Roelofs, B. Mei, I. Chorkendorff, S. F. Bent, P. C. K. Vesborg, *ACS Appl. Mater. Interfaces* **2016**, *8*, 14301–14306.

[21] T.-B. Song, Q. Chen, H. Zhou, C. Jiang, H.-H. Wang, Y. Yang, Y. Liu, J. You, Y. Yang, *J. Mater. Chem. A*, **2015**, *3*, 9032–9050.

[22] P. You, Z. Liu, Q. Tai, S. Liu and F. Yan, *Adv. Mater.,* **2015**, *27*, 3632–3638.

[23] C. Rold´an-Carmona, O. Malinkiewicz, R. Betancur, G. Longo, C. Momblona, F. Jaramillo, L. Camacho and H. J. Bolink, *Energy Environ. Sci.,* **2014**, *7*, 2968–2973.

[24] C. O. Ramirez Quiroz, I. Levchuk, C. Bronnbauer, M. Salvador, K. Forberich, T. Heumuller, Y. Hou, P. Schweizer, E. Spiecker and C. J. Brabec, *J. Mater. Chem. A,* **2015**, *3*, 24071–24081.

[25] L. Yuan, Z. Wang, R. Duan, P. Huang, K. Zhang, Q. Chen, N. K. Allam, Y. Zhou, B. Song, and Y. Li *J. Mater. Chem. A*, **2018**, *6*, 19696–19702.

[26] G. E. Eperon, D. Bryant, J. Troughton, S. D. Stranks, M. B. Johnston, T. Watson, D. A. Worsley and H. J. Snaith, *J. Phys. Chem. Lett.,* **2015**, *6*, 129–138.

[27] G. E. Eperon, V. M. Burlakov, A. Goriely and H. J. Snaith, *ACS Nano*, **2014**, *8*, 591–598.

[28] J. H. Heo, M. H. Jang, M. H. Lee, H. J. Han, M. G. Kang, M. L. Lee and S. H. Im, *J. Mater. Chem. A,* **2016**, *4*, 16324–16329.

[29] Y. Guo, K. Shoyama, W. Sato and E. Nakamura, *Adv. Energy Mater.,* **2016**, *6*, 1502317.

[30] S. Xiao, H. Chen, F. Jiang, Y. Bai, Z. Zhu, T. Zhang, x. Zheng, G. Qian, C. Hu, Y. Zhou, Y. Qu and S. Yang, *Adv. Mater. Interfaces,* **2016**, *3*, 1600484.

[31] Y. B. Yuan, P. Sharma, Z. G. Xiao, S. Poddar, A. Gruverman, S. Ducharme, J. S. Huang, *Energy Environ. Sci.* **2012**, *5*, 8558−8563.

[32] B. Yang, Y. B. Yuan, P. Sharma, S. Poddar, R. Korlacki, S. Ducharme, A. Gruverman, R. Saraf, J. S. Huang, *Adv. Mater.* **2012**, *24*, 1455−1460.

[33] N. Lin, J. Qiao, H. Dong, F. Ma, L. Wang, *J. Mater. Chem. A,* **2015***, 3*, 22839–22845.

[34] K. S. Nalwa, J. A. Carr, R. C. Mahadevapuram, H. K. Kodali, S. Bose, Y. Chen, J. W. Petrich, B. Ganapathysubramanian, S. Chaudhary, *Energy Environ. Sci.* **2012**, *5*, 7042−7049.

[35] M. B. Islam, M. Yanagida,Y. Shirai, Y. Nabetani, K. Miyano, *Solar Energy Materials and Solar Cells,* **2019**, *195*, 323-329.

[36] S. Zhang, Y. Lu, B. Lin, Y. Zhu, K. Zhang, N.-Y. Yuan, J.-N. Ding, B. Fang, *Sol. Ener. Mat. & Sol. Cells* **2017**, *170*, 178–186

[37] F. Fu, T. Feurer, T.P. Weiss, S. Pisoni, E. Avancini, C. Andres, S. Buecheler, A.N. Tiwari, *Nat. Energy* **2016**, *2*, 16190.

[38] J.H. Noh, S.H. Im, J.H. Heo, T.N. Mandal, S.I. Seok, *Nano Lett.* **2013**, *13*, 1764 1769.

[39] Y. Z. Wu, A. Islam, X. D. Yang, C. J. Qin, J. Liu, K. Zhang, W. Q. Peng, L. Y. Han, *Energy Environ. Sci.* **2014**, *7*, 2934−2938.

[40] L. Bu, Z. Liu, M. Zhang, W. Li, A. Zhu, F. Cai, Z. Zhao and Y. Zhou *ACS Appl. Mater. Interfaces* **2015**, *7*, 17776−17781.

[41] J. A. Christians, J. S. Manser, P. V. Kamat, *J. Phys. Chem. Lett.* **2015**, *6*, 852-857.

[42] Y. Lin, Y. Fang, J. Zhao, Y. Shao, S. J. Stuard, M. M. Nahid, H. Ade, Q. Wang, J. E. Shield, N. Zhou, A. M. Moran & J. Huang, *Nat. Comm.* **2019**, *10*, 1008.

[43] M. Salado, S. Kazim, M. K. Nazeeruddin and S. Ahmad, *ChemSusChem* **2019**, *12*, 2366-2372.

[44] L. C.-Bernal, M. Salado, A. Todinova, L. Calio, S. Ahmad, J. Idígoras, and J. A. Anta, *J. Phys. Chem. C*, **2017**, *121*, 9705–9713.
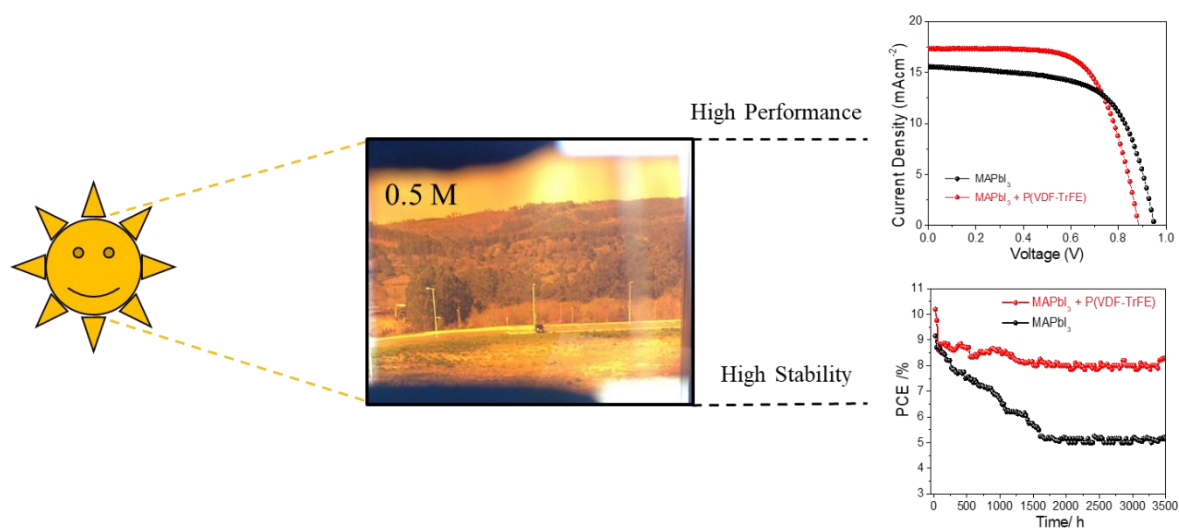
Table of content [TOC]

Image illustrating the semi-transparent perovskite solar cells for building integrated application with improved stability.

Supporting Information

Polymer amplification to improve performance and stability towards semi-transparent perovskite solar cells fabrication

Hafez Nikbakht [a,d†], Ahmed Esmail Shalan [a†], Manuel Salado [a], Abbas Assadi [c], Parviz Boroojerdian [d] Samrana Kazim,[a,b] and Shahzada Ahmad,[a,b]*

[a] BCMaterials-Basque Center for Materials, Applications and Nanostructures, Martina Casiano, UPV/EHU Science Park, Barrio Sarriena s/n, Leioa 48940, Spain.

Tel: +34 946128811 Email: shahzada.ahmad@bcmaterials.net

[b] IKERBASQUE, Basque Foundation for Science, Bilbao, 48013, Spain.

[c] School of Mechanical Engineering, Maleke-Ashtar University of Technology (MUT), Isfahan 83145, Iran

[d] Department of Applied Physics, Maleke-Ashtar University of Technology (MUT), Shahin Shahr 83157-13115, Iran

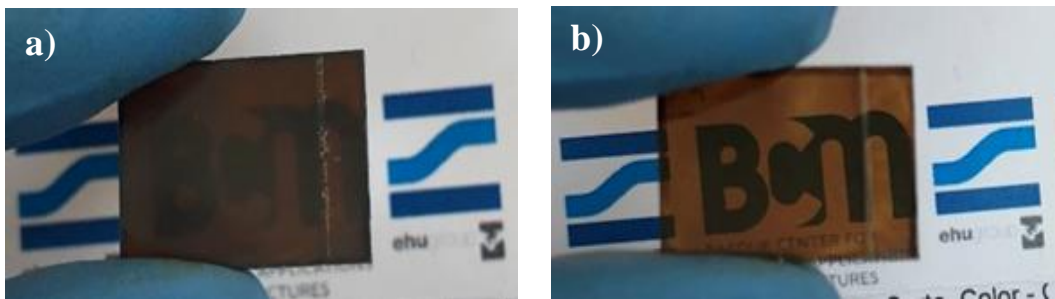[†] Authors contribute equally to the manuscript

Figure S1: Visual picture of the perovskite layer with a) 1.2M precursor concentration and b) with 0.5 M precursor concentration with P(VDF-TrFE). The latter showing the semi-transparent behaviour can be used for BIPV application.
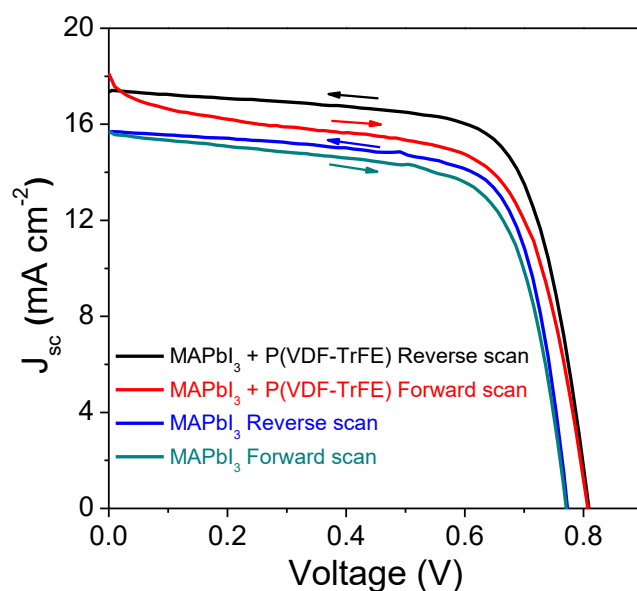

Figure S2: The forward and reverse direction $J-V$ curves of MAPbI$_3$ and with P(VDF-TrFE) based PSCs. Note the forward direction was measured after 3500 hours.
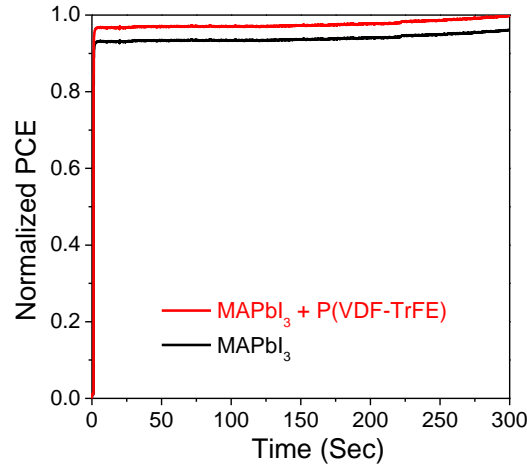
Figure S3: Normalized PCE at maximum power point tracking for pristine 0.5M MAPbI$_3$ and with P(VDF-TrFE) for 300 s.
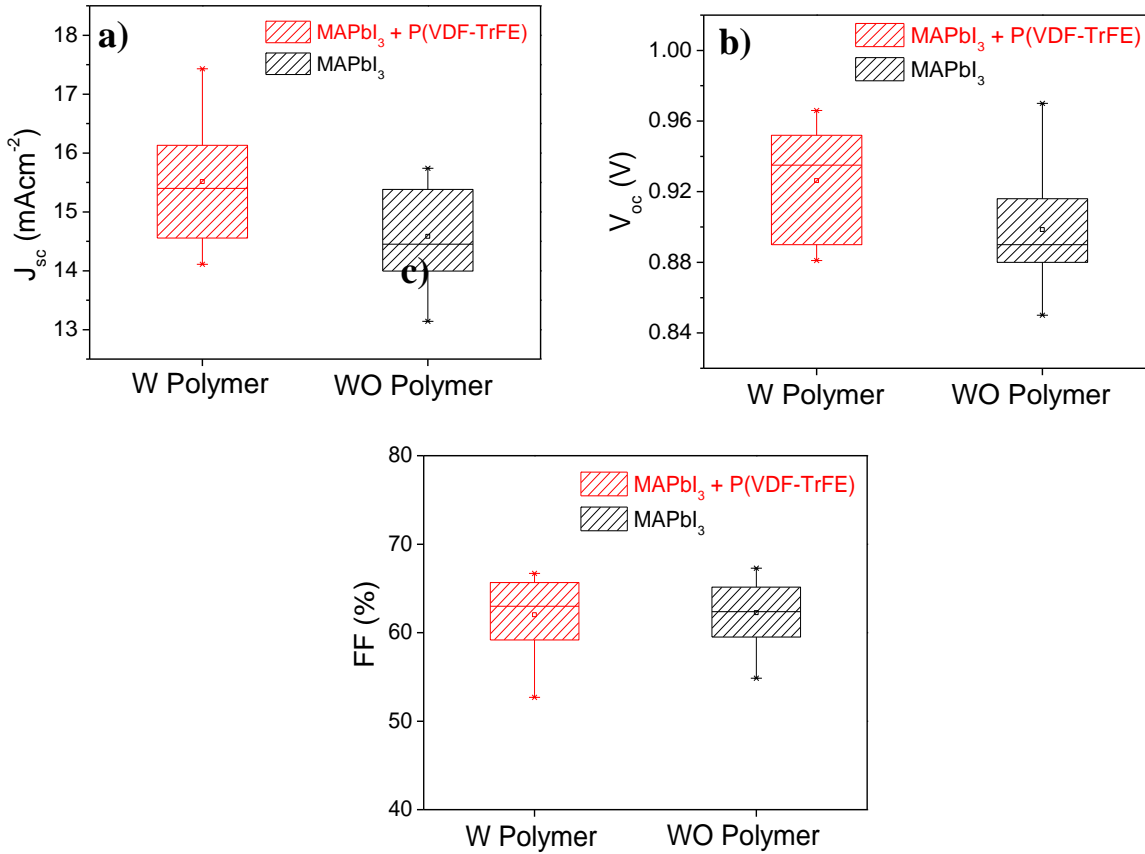

Figure S4: Statistical analysis in box charts form for a) J_{sc}, b) V_{oc}, and c) FF for perovskite solar cells with and without polymer P(VDF-TrFE).
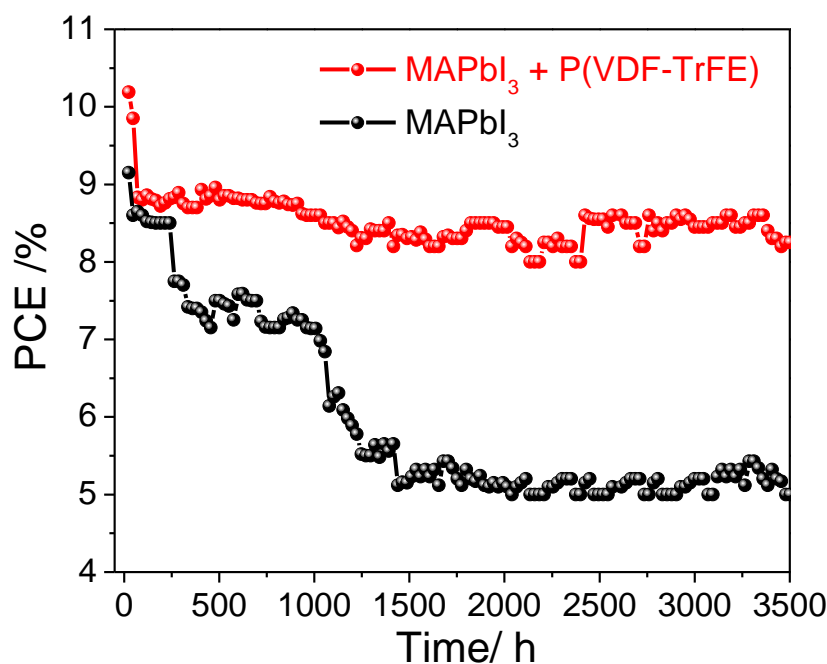
Figure S5: Performance of the fabricated solar cells PCE, monitored periodically with pristine MAPbI$_3$ and with P(VDF-TrFE). The devices were kept under controlled condition (inside the glovebox).
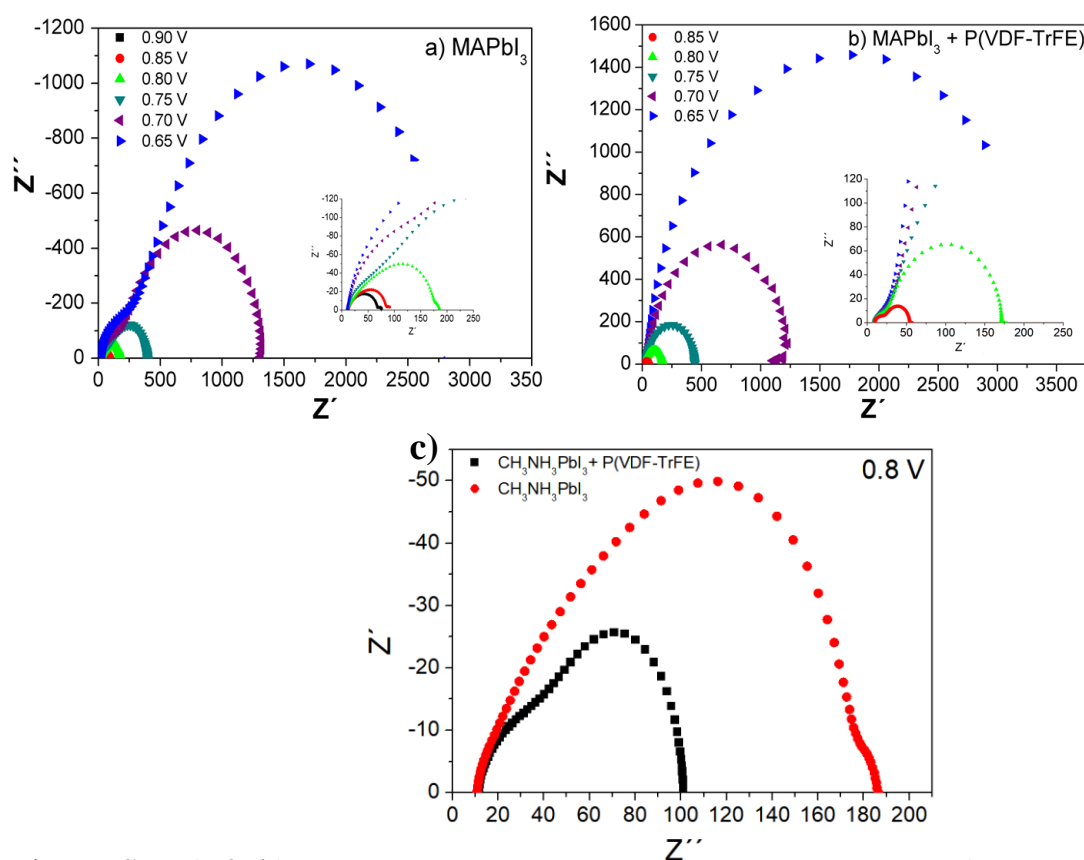

Figure S6: a) & b) Nyquist plot of pristine MAPbI$_3$ and with P(VDF-TrFE) and c) Nyquist plot comparing both material at 800mV close to the open circuit voltage.

Table S1: Photovoltaic parameters (J_{sc}, V_{oc}, *FF* and *PCE)* in reverse and forward direction for fabricated PSCs based on 0.5 M precursor perovskite solution and with *P(VDF-TrFE)*.

Devices[a]		J_{SC} /mA cm^{-2}	V_{OC} /mV [b]	FF [b]	PCE%[b]
MAPbI$_3$ + P(VDFTrFE) (Reverse Scan)		17.44	808	0.707	9.98
MAPbI$_3$ + P(VDFTrFE) (Forward Scan)		17.05	806	0.642	9.10
MAPbI$_3$ (Reverse Scan)		15.70	773	0.716	8.69
MAPbI$_3$ (Forward Scan)		15.61	771	0.685	8.25

[a] The devices were fabricated using perovskite solution (0.5M concentration) with and without polymer P(VDF-TrFE). Note the forward direction was measured after 3500 hours.

Table S2. Photovoltaic parameters of PSCs devices fabricated from 0.5M concentration perovskite solution with P(VDF-TrFE), under simulated AM-1.5G illumination (power density 100 mW cm^{-2}) with active area 0.16 cm^2.

Number of cells	J_{sc}(mA/cm^2)	V_{oc} (V)	FF (%)	PCE (%)
1	17.34	0.885	66.44	10.2
2	16.25	0.952	62.98	9.74
3	15.65	0.952	63.24	9.42
4	15.25	0.952	62.98	9.15
5	15.68	0.898	64.83	9.13
6	16.64	0.922	60.11	9.23
7	17.27	0.887	63.18	9.69
8	14.33	0.936	65.16	8.76
9	14.11	0.949	61.25	8.21
10	14.45	0.966	59.28	8.28
11	15.09	0.963	56.23	8.17
12	14.95	0.944	58.68	8.28
13	17.43	0.934	52.69	8.58
14	15.75	0.928	66.16	8.83
15	14.26	0.881	66.69	8.44
16	14.59	0.89	66.27	8.6
17	15.55	0.966	57.15	8.59
18	16.01	0.89	59.06	8.44
19	15.16	0.94	61.66	8.81
20	14.52	0.89	66.4	8.65
Average	15.51±1.04	0.93±0.031	62.02±3.94	8.86±0.57

Table S3. Photovoltaic parameters of PSCs devices fabricated from pristine 0.5 M concentration perovskite solution, under simulated AM-1.5G illumination (power density 100 mW cm^{-2}) with active area 0.16 cm^2.

Number of cells	J_{sc}(mA/cm^2)	V_{oc} (V)	*FF* (%)	PCE (%)
1	15.25	0.952	62.98	9.15
2	13.34	0.897	62.2	7.45
3	13.61	0.884	59.19	7.13
4	15.7	0.85	54.86	7.5
5	14.87	0.893	65.38	8.69
6	15.3	0.902	64.92	8.98
7	14.32	0.879	62.44	7.86
8	14.43	0.934	62.69	8.45
9	14.47	0.89	62.31	7.98
10	13.97	0.93	59.13	7.7
11	14.8	0.89	61.14	8.05
12	15.55	0.96	57.12	8.42
13	13.65	0.88	66.38	8.01
14	14.1	0.89	65.93	8.29
15	15.74	0.88	59.82	8.29
16	14.02	0.88	67.28	8.34
17	14.22	0.88	67.03	8.47
18	13.14	0.86	64.89	7.41
19	15.72	0.97	57.88	8.79
20	15.46	0.87	61.72	8.37
Average	14.58±0.84	0.90±0.033	62.26±3.48	8.17±0.54